catalysts

MDPI

Article

Synergy Effects of Cobalt Oxides on Ni/Co-Embedded Al_2O_3 for Hydrogen-Rich Syngas Production by Steam Reforming of Propane

Kyung Soo Park, Min Hye Jeong and Jong Wook Bae *

School of Chemical Engineering, Sungkyunkwan University (SKKU), 2066 Seobu-ro, Jangan-gu, Suwon 16419, Korea; ksupark91@skku.edu (K.S.P.); elpure0230@skku.edu (M.H.J.)

* Correspondence: finejw@skku.edu; Tel.: +82-31-290-7347

Received: 29 March 2020; Accepted: 22 April 2020; Published: 24 April 2020

Abstract: The synergetic effects of Co oxides on the Ni/CoAl (NCA) catalysts were observed at an optimal molar ratio of Al/Co = 2 (NCA(2)) due to the partial formations of thermally stable spinel $CoAl_2O_4$ phases for the steam reforming of propane (SRP). The optimal content of the spinel $CoAl_2O_4$ phases on the NCA(2) was responsible for the formation of the relatively active oxophilic metallic Co nanoparticles with a smaller amount of less active $NiAl_2O_4$ on the surfaces by preserving the relative amount of metallic Co of 68% and 52% in the reduced and used catalysts, which enhanced the catalytic activity and stability with the largest specific rate of 1.37 $C_3H_8/(Ni + Co)h^{-1}$ among the tested NCA catalysts. The larger or smaller amounts of Co metal on the less active NCA mainly caused the preferential formation of larger aggregated Ni nanoparticles ~16 nm in size due to their weaker interactions, or induced the smaller formations of active metal phases by selectively forming the spinel $NiAl_2O_4$ phases with ~60% in the NCA(4), resulting in a fast deactivation.

Keywords: steam reforming of propane (SRP); Ni nanoparticles; spinel $CoAl_2O_4$ and $NiAl_2O_4$; metal–support interaction; synergetic effect

1. Introduction

Hydrogen has been remarkably spotlighted recently as clean energy due to its high efficiency with low emissions of greenhouse gases through a fuel cell application compared to conventional fossil fuel-based energies [1]. Moreover, since the emission regulations are getting stricter in regard to not only power generation but also vehicles, the needs of clean fueled vehicles, such as electric or fuel cell vehicles, are more attractive compared to the conventional fossil fuel combusting vehicles. For the fuel cell applications, hydrogen can be generally produced from a fuel processing technology composed of the following units; desulfurization, steam reforming, water-gas shift and preferential oxidation of carbon monoxide, which could convert hydrocarbons to hydrogen-rich gas with sparse CO concentration. Among those hydrocarbons, propane can be one of the promising feedstocks for the fuel processor since it can be easily liquified at room temperature, resulting in easy shipping and transportation compared to other gaseous feedstocks [2]. Therefore, the existing infrastructures can be directly utilized to supply the feedstock for the fuel processor applications. The steam reforming of light alkanes, which is the most economical way to produce the industrially applicable hydrogen, typically takes about 60% market share among overall hydrogen production plants due to its relatively stable syngas production as well as high H_2/CO ratio compared to other various reforming processes [3]. Steam reforming of propane (SRP) is mainly composed of the reactions as listed below.

$$\text{Steam reforming of propane (SRP): } C_3H_8 + 3H_2O \rightarrow 3CO + 7H_2 \ (\Delta H^\circ = 497.7 \text{ kJ/mol}) \quad (1)$$

$$\text{Water-gas shift reaction (WGS): } CO + H_2O \leftrightarrow CO_2 + H_2 \ (\Delta H^\circ = -41.1 \text{ kJ/mol}) \quad (2)$$

$$\text{Steam reforming of methane (SRM): } CH_4 + H_2O \leftrightarrow CO + 3H_2 \ (\Delta H^\circ = 205.9 \text{ kJ/mol}) \quad (3)$$

$$\text{Boudouard reaction: } 2CO \leftrightarrow CO_2 + C \ (\Delta H^\circ = -172.4 \text{ kJ/mol}) \quad (4)$$

For the production of hydrogen-rich syngas, it is essential to promote WGS and SRM to boost H_2 production and to suppress CO formation simultaneously [4]. Although propane can be easily decomposed in the operation temperatures of 500–800 °C due to its highly endothermic and irreversible natures in thermodynamics with their faster rates, there are not only the reforming reaction but also thermolysis at high temperature, which largely generating solid carbons under the reaction conditions compared to the SRM reaction [5]. Furthermore, since carbon depositions generally originate from Boudouard reactions and thermal hydrocarbon decompositions during the processes, more delicate efforts should be endeavored to maintain the stable catalytic activity [6–8].

The group VIII noble metals such as Rh, Pt, Ru, Pd and Ir-based reforming catalysts have been widely used due to their remarkable catalytic activities for hydrocarbon reforming processes with insignificant coke formations [7,9–11]. However, their costs are relatively high, therefore they are scarcely allowed in industries compared to Ni-based reforming catalysts, which have comparable catalytic activities to the noble metal-based ones. One of the critical disadvantages of the Ni-based catalysts is their thermal instability which induces severe aggregations of the active Ni nanoparticles during the high temperature reforming reaction. In addition, the solid carbons are easily deposited, causing the significant catalyst deactivation. Moreover, the facile aggregations of Ni metals, which lead to their transformations to the less active solid-solutions such as nickel aluminates, induce lower stability of the Ni-based catalysts [12,13]. The Ni-based reforming catalysts can be modified to lessen these problems by following general methodologies: to keep the small sizes of nickel nanoparticles [14–17] for better dispersion and less aggregation, to modify the supports via addition of alkali metals, lanthanides and rare earth metals [5,18–22], to decrease carbon deposition with a help of basicity of those promoters and to add a small amount of noble metals such as Ru and Rh to promote the in-situ reducibility of the Ni species through various synthetic methods [9,23]. Interestingly, compared to the monometallic Ni or Co-based catalysts, bimetallic catalysts using Ni and Co species simultaneously were reported to enhance the catalytic performances as well as produce less coke formations in various reforming processes [12,24–26]. These synergetic effects generally originated from the formations of the Ni-Co alloy which made the higher electron density in metallic Ni, enhancing the reforming activity and the resistances to sintering and coking as well [25]. It was also reported that the oxophilic Ni-Co clusters can activate the oxidants of CO_2 and H_2O, which are able to gasify the solid surface carbon easily [26]. However, it is still under debate whether the synergetic effects came from a bimetal alloy or independent metallic clusters with their enhanced dispersions affected by the impurities during the reduction process [27]. Many hypotheses have been proposed based on the density functional theory (DFT) calculations, since Ni and Co are hardly differentiated by the X-ray techniques due to their similar crystal structures with similar atomic sizes [26].

In the present study, the surface distributions and capacity to form solid solutions was controlled on the sol-gel synthesized Co_3O_4-Al_2O_3 (CA) supports with different Al/Co ratio to figure out the synergetic effects of Ni-Co combination on the Ni/Co-embedded Al_2O_3 (NCA) catalysts for the superior catalytic performances during the SRP reaction. The relative amounts of metal (oxide) phases and their distributions were characterized to figure out an optimal Al/Co ratio to balance the crystallite sizes of the metallic Co species with its natures, to form thermally stable spinel $CoAl_2O_4$ and $NiAl_2O_4$ phases by maximizing the synergetic effects through the different formations of those solid solutions.

2. Results

2.1. Physicochemical Properties of NCA Catalysts

The physicochemical properties of the as-prepared NCA catalysts are summarized in Table 1 by explaining the elemental compositions, textural properties, crystalline sizes and dispersion of active metals. The intended nominal amount of active Ni species was successfully impregnated on the NCA catalysts, where the NiO contents were found to be in the range of 10 wt–12 wt% from X-ray fluorescence (XRF) analysis. Relative amounts of Co_3O_4 and Al_2O_3 were changed from 64.3 wt–22.6 wt% and 24.8 wt–66.2 wt% in accordance with the molar ratios of Al/Co from 0.5 to 4. Accordingly, the specific surface areas and pore volumes were increased from 32 to 111 m^2/g and 0.24 to 0.48 cm^3/g as displayed in Table 1 and Figure S1A due to the increased mesopore structures of Al_2O_3 with typical type IV isotherms [28]. Average pore diameters of the NCA catalysts were found to be larger than 10 nm, which suggests that most of the mesopore structures originate from their inter-particular pores of the Co-Al mixed oxide grains, and the average pore diameters were decreased with an increase of the Al/Co ratio due to larger contributions of Co_3O_4-Al_2O_3 porosity (Figure S1B).

Table 1. Bulk and surface properties of the Ni/CoAl (NCA) catalysts prepared at different Al/Co ratios.

Notation	XRF (wt%)			N_2-Sorption [1]			XRD	CO Chemi.
	NiO	Co_3O_4	Al_2O_3	S_g (m^2/g)	P_v (cm^3/g)	P_d (nm)	Crystallite Size of Ni^0 (Reduced/Used) (nm)	Dispersion (%)
NCA(0.5)	10.9	64.3	24.8	32	0.24	25.2	14.6/16.2	1.0
NCA(1)	10.6	50.6	38.8	46	0.36	27.6	9.2/12.9	2.4
NCA(2)	10.3	36.1	53.6	64	0.39	20.5	6.9/8.7	2.5
NCA(3)	11.9	28.4	59.7	78	0.43	15.3	6.3/7.4	3.6
NCA(4)	11.2	22.6	66.2	111	0.48	12.9	6.5/7.3	3.0

[1] S_g, P_v and P_d represent the specific surface area (m^2/g), pore volume (cm^3/g) and average pore diameter (nm) measured by N_2 adsorption-desorption analysis on the fresh NCA catalysts, respectively.

The increased amounts of cobalt metal on the NCA catalysts caused the decreased surface area due to the increased crystallite sizes and small contributions of mesoporous Al_2O_3, which were calculated by using the main diffraction peaks detected in the range of 44.2° for Co (111)–44.5° for Ni (111) with the help of the Scherrer equation as shown in Figure 1 and Figure S2. The metallic Ni crystallite sizes were found to be 6.5 nm on NCA(4) and 14.6 nm on NCA(0.5), which were decreased with an increase of the Al/Co ratio. It is worth noting that NCA(3) and NCA(4) had the smallest crystallite sizes of 6.3–6.5 nm (dispersion of 3.0–3.6%) among the reduced NCA catalysts. In addition, the characteristic diffraction peaks assigned to the spinel-type $NiAl_2O_4$, Co_3O_4 and $CoAl_2O_4$ phases were observed at 31°, 37°, 45°, 56°, 59° and 65°, which are scarcely classified due to their overlapped positions with the same crystal structures of AB_2O_4 [7,22,29–32]. Diffraction peaks assigned to the γ-Al_2O_3 phases were also observed, with their smaller peaks at 38°, 46° and 67°, which also suggests that the Al_2O_3 seems to exist mainly in the spinel-types such as $NiAl_2O_4$ and $CoAl_2O_4$ in the NCA catalysts [12,33]. Interestingly, the peaks of the main diffraction at 44.2°–44.5° were shifted to the higher two theta values and broadened with a decrease of cobalt contents, especially on the NCA(3) and NCA(4), due to the smaller crystallite formations corresponding to larger surface areas. Even though those peaks were hard to be assigned to the different crystalline phases, the transformations of those major crystallite structures were observed from the metallic Co and Ni to the spinel-type $NiAl_2O_4$ and $CoAl_2O_4$ phases at higher Al/Co ratios on the reduced NCA catalysts (Figure 1A). After the SRP reaction at 650 °C, the used NCA catalysts showed increased metallic crystallite sizes (Figure 1B) due to the aggregations of those nanoparticles with their sizes of 7.3–16.2 nm from 6.3–14.6 nm, as summarized in Table 1. The extents of the aggregations were not significant on the NCA catalysts with a Al/Co ratio ≥2, such as the NCA(3) and NCA(4), while the much bigger crystallites were formed on the used NCA(1) and NCA(0.5) to 12.9 and 16.2 nm in size, respectively. The moderate aggregations of Ni nanoparticles on the NCA(2) (from 6.9 to 8.7 nm with dispersion of 2.5%) were mainly attributed to the formations of

strongly interacted Co_3O_4-Al_2O_3 particles with a moderate surface area (64 m^2/g), which can be more beneficial for increasing the catalytic activity and stability.

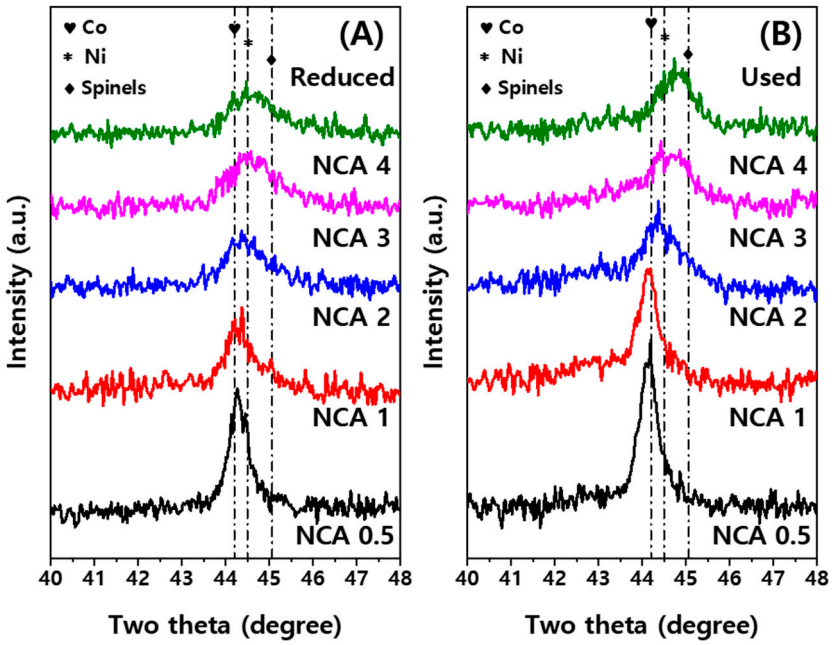

Figure 1. X-ray diffraction patterns of the (**A**) reduced and (**B**) used NCA catalysts.

2.2. Reduction Properties of NCA Catalysts and Catalytic Activities of CA Supports Themselves

As shown in Figure 2A, the reduction behaviors of the NCA catalysts were measured by temperature programmed reduction (TPR) analysis. With lower contents of cobalt species on the NCA(3) and NCA(4), one reduction peak at the respective temperatures of 842 and 854 °C was clearly observed. In general, cobalt-promoted Ni-based catalysts show the lower temperature shifts of those reduction peaks by facilitating an easy reduction of Ni/Al_2O_3 [12] as observed in Figure 2A from 854 °C on the NCA(4) to 833 °C on the NCA(0.5). In case of the Al/Co ≥ 3, the higher temperature reduction peaks above 800 °C were mainly attributed to the reduction of solid solutions, such as the spinel $CoAl_2O_4$ and $NiAl_2O_4$ (or strongly interacted NiO species), which were scarcely reduced below 700 °C to metallic Co and Ni due to their stronger metal–support interactions [3,12,25]. With the decreases of Al/Co ratios below two, many additional reduction peaks were observed with broader reduction patterns below 800 °C, which originated from the stepwise reductions of spinel-type oxides [12,13,19,31] such as $CoAl_2O_4$, Co_3O_4 and $NiAl_2O_4$. In detail, the apparent reduction peaks of cobalt oxides through stepwise reductions ($Co_3O_4 \rightarrow CoO \rightarrow Co$) were clearly observed below 700 °C, which suggests the preferential segregations of the active cobalt species were on the outer surfaces of the NCA(0.5) and NCA(1) compared to the supports themselves (CA(0.5) and CA(1)) which have lower activity for SRP reactions as well. Interestingly, on the NCA(2), the smaller segregated cobalt species (below ~700 °C) as well as spinel-type metal oxides (at ~839 °C) were observed, which were responsible for an enhanced catalytic activity and stability through the formation of thermally stable mixed metal interfaces.

The catalytic activity of the CA supports and NCA(1) with an impregnated Ni/Al_2O_3 and $CoAl_2O_4$ reference catalysts were preliminarily measured at a lower SV = 100,800 L/(kg_{cat}·h), and the results are displayed in Figure 2B and summarized in Table S1. The CA supports themselves were active for the SRP reaction without any Ni species, which suggests that the cobalt nanoparticles were active for the reaction [3,25,34]. It was clear that the CA supports with the molar ratio of Al/Co ≤ 2 were also active for SRP reaction, and their higher and stable activities were characterized compared to the reference catalysts of Ni/Al_2O_3 and $CoAl_2O_4$. In addition, the CA supports were highly stable compared to the Ni/Al_2O_3, which was gradually deactivated for five hours at 550 °C from 51.4% to

42.8% due to possible coke depositions at a relatively low temperature [35,36]. With an increased Co content, the catalytic activity was still higher on the CA(1) and CA(0.5) with the C_3H_8 conversion of 57.4 and 57.2%, while the CA(1) was more active than the CA(0.5) above 650 °C (respective values of 79.6% and 86.9% at 650 °C), which was attributed to the preferential aggregations of Co particles on the CA(0.5). Interestingly, an impregnation of Ni metal on the NCA(1) catalyst revealed a 100% conversion of C_3H_8 at all temperatures from 550 to 750 °C without any deactivation phenomena. This observation revealed an extraordinary activity compared to the reference Ni/Al_2O_3, owing to the synergetic effects of Ni and Co [3,12,25]. However, the CA supports with Al/Co ≥ 3 and commercially available spinel $CoAl_2O_4$ were not active below 650 °C since there could be little metallic Co nanoparticles even after reduction step due to their stronger metal–support interactions [37].

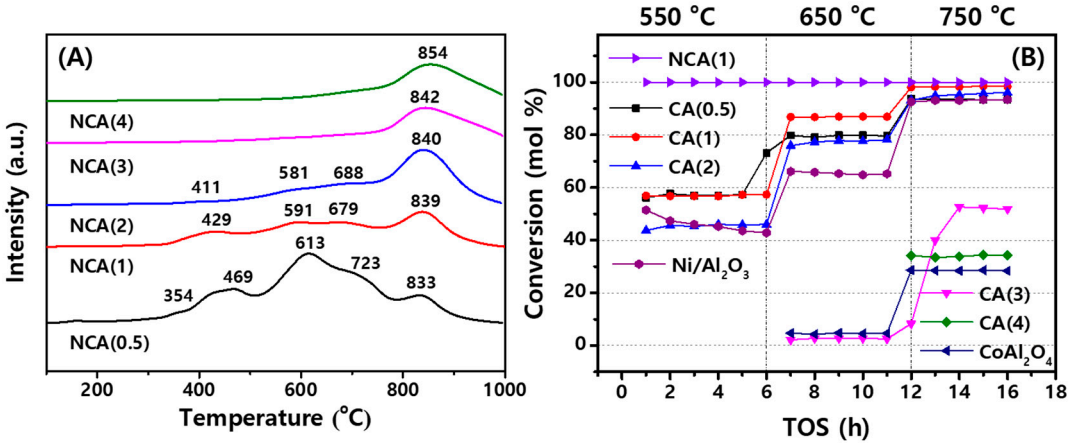

Figure 2. (**A**) Reduction behaviors of the NCA catalysts measured by temperature programmed reduction (TPR) analysis, (**B**) Results of preliminary activity measurement of the Co_3O_4-Al_2O_3 (CA) supports with reference samples such as Ni/Al_2O_3 and $CoAl_2O_4$ for C_3H_8 conversion with time on stream (h) at the reaction condition of T = 550–650–750 °C, P = 0.1 MPa and SV = 100,800 L/(kg_{cat}·h) by using a feed gas composition of $C_3H_8/N_2/H_2O$ = 1:4:9.

2.3. Catalytic Activities of NCA Catalysts with Coke Analysis

The SRP reaction was carried out again on the NCA catalysts at a slightly higher space velocity of 170,000 mL/g_{cat}·h with the mixed gas composition of $C_3H_8/N_2/H_2O$ = 1/4/9 at a fixed temperature of 650 °C, and the results of C_3H_8 conversion and its specific rate (C_3H_8 converted/(moles of (Ni + Co)·h)) are respectively displayed in Figure 3A,B. As summarized in Table 2, the conversions of C_3H_8 were steadily increased with the decrease of Al/Co ratio, such as 49.5% on the NCA(4) and 78.1% on to NCA(1), except for the structurally unstable NCA(0.5). Based on the preliminary tests of the CA supports, the metallic Co species on the CA supports with a lower Al/Co ratio such as NCA(1) and NCA(2) seem to promote the reforming activity through the synergetic effects of Ni nanoparticles due to its own catalytic activity of the surface metallic Co nanoparticles. However, the NCA(0.5) with the largest amount of Co metal showed a continuous activity decrease from an initial conversion of 83.0% to 73.2% and larger deactivation rate of 0.89%/h due to the severe aggregations of the active Ni and Co nanoparticles with the variations of Ni size from 14.6 to 16.2 nm during SRP reaction measured by X-ray diffraction (XRD) analysis (Table 1). The optimal NCA(1) and NCA(2) showed the moderate propane conversions of 72.6–78.1% with smaller deactivation rates of 0.27–0.31%/h while the NCA(4) showed the lowest conversion (49.5%) due to the small amount of active cobalt metal content with its less synergetic effects, which was confirmed by TPR analysis of the CA supports (Figure 2). However, the specific rates, defined as [converted mols of C_3H_8 divided by the moles of Ni and Co metals per hour], revealed the lower rate of 0.96 on the NCA(0.5) (largest metal content) with larger metal aggregates with smaller active sites [20] and higher rate of 1.37 on the NCA(2) even though the metal particles on the NCA(2) were aggregated during the SRP reaction. This suggests that the Ni and Co

metals have some additional synergy effects through the proper distributions of the active metallic Co nanoparticles on the NCA surfaces as well as optimal formations of the thermally stable spinel $CoAl_2O_4$ and $NiAl_2O_3$ phases on the bulk CA(2) support [12,32,33,37], as explained in the following section. In addition, the highly reduced NCA(0.5) and NCA(1) revealed a slightly lower H_2 selectivity of 70.1–71.2% and higher CH_4 selectivity of 4.4–5.2% compared to the less reduced NCA(2) with those values of 73.2% and 2.0%, which can be possibly attributed to the more preferential methanation activity as well as coke depositions by possibly inducing the smaller contributions of SRM activity on the metallic Co and Ni surfaces [4–8,33].

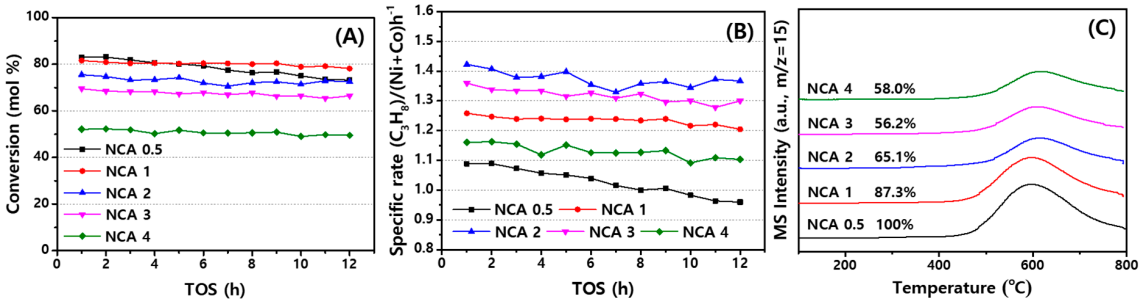

Figure 3. Catalytic activities of the NCA catalysts for (**A**) C_3H_8 conversion, (**B**) specific rate of C_3H_8 conversion (C_3H_8 converted/(moles of (Ni + Co)·h)) with time on stream (h) and (**C**) Temperature programmed surface reaction (TPSR) patterns of the used NCA catalysts at the reaction conditions of T = 650 °C, P = 0.1 MPa and SV = 170,000 L/(kg_{cat}·h) by using a feed gas composition of $C_3H_8/N_2/H_2O$ = 1:4:9.

Table 2. Summarized results of the catalytic performances on the NCA catalysts.

Notation	Catalytic Performances [1]			
	Conversion (mol%)	Specific Rate [Moles of C_3H_8 Converted/(Moles of (Ni + Co)·h)]	Deactivation Rate (%/h)	Product Distribution (H_2/CO/CO_2/CH_4)
NCA(0.5)	73.2	0.96	0.89	71.2/8.6/15.8/4.4
NCA(1)	78.1	1.20	0.31	70.1/9.0/15.7/5.2
NCA(2)	72.6	1.37	0.27	73.2/8.5/16.3/2.0
NCA(3)	66.5	1.30	0.28	72.5/7.6/16.8/3.1
NCA(4)	49.5	1.10	0.23	73.4/10.6/14.1/1.9

[1] SRP reaction was performed at the reaction conditions of T = 650 °C, P = 0.1 MPa and SV = 170,000 L/(kg_{cat}·h) by using a feed gas composition of $C_3H_8/N_2/H_2O$ = 1:4:9 for 12 h on stream. The extent of deactivation (%/h) was the difference between the initial and final conversion of C_3H_8 divided by 11 h, and all values such as conversion, specific rate and product distribution were included by using the final catalytic activity at 12 h.

The surface coke types and their relative amounts on the used NCA catalysts were characterized by temperature programmed surface reaction (TPSR), and TPSR patterns monitored with a mass spectrometer (CH_4 fragment, m/z = 15) are displayed in Figure 3C, including their relative intensity ratio based on that of NCA(0.5). There were insignificant amounts of soft coke precursors formed on the NCA catalysts, which can be hydrogenated to CH_4 at low temperature of ~300 °C, however, hard coke precursors detected at the temperature regions of 550–800 °C [38] were mainly observed on all the used NCA catalysts. The hydrogenation peak positions at ~600 °C shifted to higher temperatures with an increase of the Al/Co ratio, which was possibly attributed to the formations of much stronger interacting, harder cokes on the Al_2O_3-rich surfaces [32,33]. In addition, the relative amounts of those hard coke precursors were found to be decreased with an increase of Al/Co ratios, being especially smaller on the NCA(2) and NCA(3), owing to the smaller crystallites, which can be responsible for less formation of cokes since the larger metallic Ni and Co nanoparticles act as active sites for coke depositions [39].

2.4. Relative Compositions of Active Metal (Oxides) Measured by X-ray Absorption Fine Structure (XAFS) Analysis

The X-ray absorption fine structure was further carried out to quantify the compositions of crystalline phases with their oxidation states of Ni and Co metals on the reduced and used NCA catalysts by observing the absorption energy of Ni K-edge (8333 eV) and Co K-edge (7709 eV). The spectra of X-ray absorption near-edge structures (XANES) and their phase compositions are summarized in Table 3 and displayed in Figures 4 and 5. The XANES spectra and their first derivatives were fitted to quantify the crystalline phases through linear combination fitting (LCF) by comparing them with various reference samples. With a decrease of the Al/Co ratio, the amounts of metallic Ni were found to be dominant with the ratio of 0.78 and 0.55 on the reduced and used NCA(0.5) with the respective composition of the $NiAl_2O_4$ phases of 0.11 and 0.28, since the smaller amount of Al_2O_3 can suppress the formations of the spinel $NiAl_2O_4$ phases with much bigger Ni nanoparticles due to their weak metal–support interaction. With an increase of Al content, the composition of $NiAl_2O_4$ phases was significantly increased up to 0.57 and 0.60 on the reduced and used NCA(4). In addition, the observed larger compositions of the NiO and $NiAl_2O_4$ phases on the used NCA catalysts compared to that of the reduced ones can be attributed to a high temperature SRP reaction condition with excess oxidative water vapor [33].

Table 3. Crystalline compositions of the Ni and Co species on the reduced and used NCA catalysts [1].

Notation	Status	Linear Combination Fitting (LCF) Results by Using XANES Spectra							
		Ni	NiO	$NiAl_2O_4$	R-Factor (%)	Co	CoO	$CoAl_2O_4$	R-Factor (%)
NCA(0.5)	Reduced	0.78	0.12	0.11	0.2	0.82	0.07	0.11	0.3
	Used	0.55	0.17	0.28	0.9	0.69	0.07	0.25	0.2
NCA(1)	Reduced	0.57	0.26	0.16	1.0	0.73	0.08	0.20	0.1
	Used	0.49	0.20	0.32	0.2	0.53	0.10	0.37	0.2
NCA(2)	Reduced	0.44	0.20	0.36	0.3	0.68	0.10	0.22	0.6
	Used	0.27	0.27	0.47	0.2	0.52	0.11	0.37	0.8
NCA(3)	Reduced	0.33	0.18	0.49	0.6	0.42	0.13	0.45	0.4
	Used	0.25	0.23	0.52	0.1	0.21	0.08	0.70	1.4
NCA(4)	Reduced	0.21	0.22	0.57	0.4	0.40	0.12	0.48	0.5
	Used	0.15	0.25	0.60	0.2	0.13	0.17	0.70	1.0

[1] X-ray adsorption fine structure (XAFS) experiment were performed at the 7D1 beam line of the Pohang Light Source (PLS) by measuring at the Ni K-edge (8333 eV) and Co K-edge (7709 eV), and the linear combination fittings (LCF) from the X-ray absorption near-edge structure (XANES) regions on the reduced and used NCA catalysts were carried out by comparing them with various reference materials. The Co_3O_4 phases was not observed on the NCA catalysts.

The relative composition of Co species also clearly showed the oxidation states as well as their distributions on the NCA catalysts according to Al/Co ratios. The distributions of Co phases were found to be similar with that of the Ni nanoparticles, where the metallic Co species was decreased with the increasing Al/Co ratio from 0.82 on the reduced NCA(0.5) to 0.40 on the reduced NCA(4) and the content of metallic Co was decreased to 0.69 on the used NCA(0.5) to 0.13 on the used NCA(4) due to an in-situ oxidation during the SRP reaction under an excess water environment. On the contrary, the content of spinel $CoAl_2O_4$ was increased with the same trends as the $NiAl_2O_4$ phases. Interestingly, the oxidation phenomena of the metallic Co to CoO and $CoAl_2O_4$ phases were possibly attributed to its facile oxidation–reduction characteristics of the oxophilic Co species [12]. Furthermore, the stable preservation of the metallic Co phases with small changes of the $CoAl_2O_4$ formation on the reduced and used NCA(2) was observed, with their changes from 0.68 to 0.52 and 0.22 and 0.37, respectively, which suggests the preservation of more stable metal phases caused the increased specific rate with less deactivation by maintaining active metallic Co and Ni phases with less coke depositions in the redox reaction condition during the SRP reaction. This was in line with the results of the TPR analysis and preliminary tests, as the amount of metallic Co was dramatically increased at lower ratios of Al/Co ≤ 2. The additional reduction peaks appearing at T $\leq$ 700 °C were responsible for the active surface

metallic Co and Ni phases for an enhanced activity for SRP reaction, which are unlike the commercially available bulk $CoAl_2O_4$ phases due to the contribution of the Co_3O_4-Al_2O_3 porosity, especially for the NCA catalysts with higher ratios of Al/Co ≥ 3. Therefore, the higher specific rate on the NCA(2) with a small deactivation rate, even though its little lower conversion of C_3H_8 compared to the NCA(1), can be attributed to the small aggregations of Ni nanoparticles on the porous Co_3O_4-Al_2O_3 surfaces due to its stronger metal–support interactions as well as small formations of less active spinel Co_3O_4 phases by robustly preserving the active metallic Co nanoparticles on the NCA(2) surfaces, even under an excess water environment.

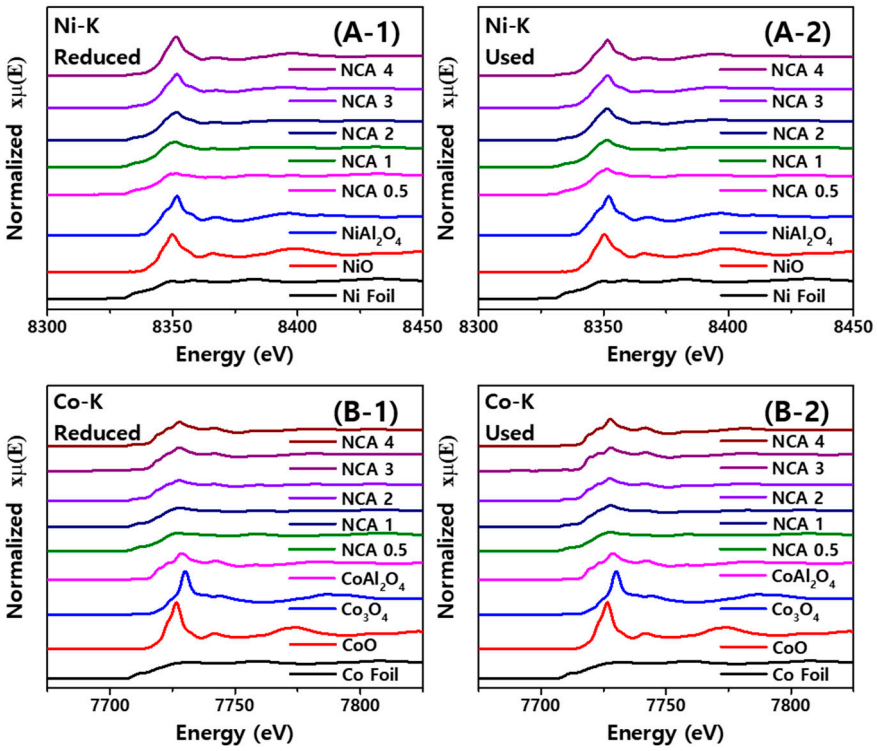

Figure 4. X-ray absorption near-edge structure (XANES) spectra of (**A**) Ni K-edge and (**B**) Co K-edge on the (**1**) reduced, (**2**) used NCA catalysts with reference materials.

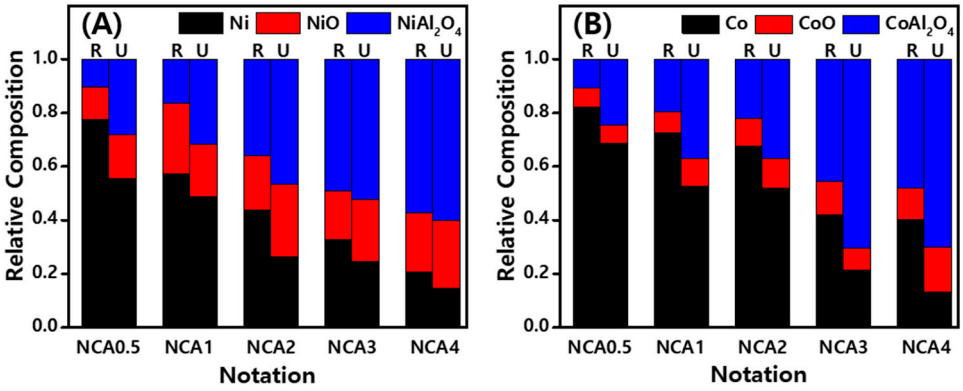

Figure 5. Relative crystalline compositions of the (**A**) reduced and (**B**) used NCA catalysts derived from the linear combination fitting (LCF) by comparing them with reference materials.

3. Discussion and Conclusions

The synergetic effects of the oxophilic Co nanoparticles for the Ni-based reforming catalysts were largely investigated in terms of the metal–support interactions and coke resistance [6,25]. In the case

of catalytic reforming reaction of hydrocarbons, it was well reported that those interactions not only enhanced the metal dispersion to promote the catalytic activity, but also lessened the coke deposition to enhance the catalytic durability. However, a lot of research was focused on simultaneously using the expensive noble metal promoters such as Rh, Ru and Pt with much cheaper Ni metal, which changed the dispersion of metal clusters, reducibility and heat of adsorption through hydrogen spillover. Those promoters can keep the Ni nanoparticles in more active metallic states by preventing the coke depositions compared to the easily deactivated monometallic Ni-based catalysts [9,23]. The bimetallic Ni-Co-based reforming catalysts were reported to possess similar promoting effects to enhance the metal dispersion and reducibility. The more interesting points of the Ni-Co-based catalysts are the oxophilic natures of the Co species, which can help increase the adsorption natures of the oxidants, such as H_2O and CO_2, by effectively preventing the coke depositions [12,26]. However, the synergetic effects of the spinel-type $CoAl_2O_4$ and $NiAl_2O_4$ formation on the Ni-impregnated Co_3O_4-Al_2O_3 (CA) support prepared at different Al/Co ratios were not well considered till now, therefore, the surface compositions of the bimetal clusters as well as contributions of spinel-type $CoAl_2O_4$ formations are briefly discussed to verify the activity variations of the home-made Ni/Co_3O_4-Al_2O_3 (NCA) catalysts for the SRP reaction.

In the present study, the synergetic effects of the Ni (fixed at ~10 wt%)and Co metal (oxides) on the CA supports, prepared by a sol-gel method with different Al/Co ratios, were verified by the characterization of the surface and bulk properties of NCA catalysts to explain the reasons for the enhanced activity and stability with their higher coke resistances on the optimal NCA(1) and NCA(2). The bulk compositions of the CA supports affected the catalytic performances largely by changing the active Ni and Co metal distributions on the porous Co_3O_4-Al_2O_3 structures and by generating the different amounts of the thermally stable spinel $CoAl_2O_4$ phases. The Co phases on the NCA catalysts were found to be mainly the metallic Co species at a lower Al/Co ratio ≤ 2 with small amounts of less active spinel $CoAl_2O_4$ phases formed under SRP reaction conditions. Those metallic Co phases were also found to be active for the SRP reaction as confirmed by preliminary tests of the CA supports by displaying better catalytic activity than the reference Ni/Al_2O_3 under the temperature of 650 °C, which was in line with the TPR results. It suggests that the cobalt oxides can be reduced to selectively form the more active metallic Co phases on the NCA(1) and NCA(2) surfaces. However, the less active $CoAl_2O_4$ phases were mainly formed on the NCA(3) and NCA(4) under an excess water environment due to their higher Al/Co ratios. Based on the XANES analysis, the partially formed bulk spinel $CoAl_2O_4$ and $NiAl_2O_4$ structures on the NCA(1) and NCA(2) can effectively enhance the thermal stability of the strongly interacted metallic Ni and Co nanoparticles with their smaller aggregation natures compared to the NCA(0.5), which was also responsible for suppressing the depositions of coke precursors. The higher specific rate of the NCA(2), with proper amounts the surface metallic Ni and Co phases with the bulk spinel $CoAl_2O_4$ phases, was attributed to the synergetic effects of the surface Ni and Co metals, as well as thermally stable bulk spinel structures.

4. Materials and Methods

4.1. Catalyst Preparation and Activity Measurement

The Co_3O_4-Al_2O_3 (CA) supports were prepared by a well-known sol-gel method by using a gelation agent of propylene oxide according to the references [12,40]. For more details, desired amounts of $Al(NO_3)_3{\cdot}9H_2O$ (Daejung, 98% purity) and $Co(NO_3)_2{\cdot}6H_2O$ (Samchun, 97% purity) were dissolved in 100 mL of anhydrous ethanol (Daejung, 99.9% purity) at fixed molar ratios of Al/Co = 0.5, 1, 2, 3 and 4 under vigorous stirring. After all the metal precursors were dissolved and well mixed, 35 mL of propylene oxide (Samchun, 99.0%) was added to the above solution as a gelation agent. The mixture was transformed into gel after 10 min under stirring followed by aging it at room temperature for 6 h. After drying at 80 °C for 60 h, the xerogel was further calcined at T = 700 °C for 3 h in an air atmosphere. The collected powder was crushed and named as CA(x), where x represents the molar ratio of Al/Co.

The Ni metal precursor was further introduced to the CA supports by a wet impregnation method at a fixed 10 wt% Ni based on the CA support. In further detail, 1.12 g of $Ni(NO_3)_2{\cdot}6H_2O$ (Samchun, above 98% purity) was dissolved in 100 mL ethanol to prepare the precursor solution. An amount of 2 g of the CA support was added to the above solution then stirred vigorously for 1 h. The solvent was evaporated at 50 °C by using a vacuum evaporator (NE-2001, EYELA). The mixture was further dried at 80 °C overnight, followed by the calcination at 700 °C for 3 h in an air atmosphere. As-prepared catalysts were denoted as NCA(x), where the x represents the molar ratio of Al/Co. For the preparation of reference catalysts, a typical Ni/Al_2O_3 catalyst was prepared by using an impregnation method with commercially available γ-Al_2O_3 (Puralox SCCa-5/170, Sasol, S_g = 165 m^2/g) support, which was further calcined at 800 °C for 2 h. The spinel $CoAl_2O_4$ was purchased from Sigma-Aldrich (cobalt aluminum oxide nano-powder with particle size < 50 nm) for the comparative activity measurement as well.

The activity measurements for steam reforming of propane (SRP) on the as-prepared NCA catalysts were performed using an Inconel fixed-bed tubular reactor with 3/8 inch of an outer diameter. An amount of 0.15 g of the NCA catalyst was placed and it was brought into contact with a thermocouple to measure the temperature gradients in the catalyst bed at a controlled furnace temperature. Prior to the SRP reaction, the catalyst was reduced at 700 °C under a flow of 50 mL/min of 5 vol% H_2/N_2 for 3 h. As the reactor was cooled down to the reaction temperature of 550 and 650 °C and stabilized, steam was fed to the reactor prior to propane feed. The SRP reaction was carried out with feed gas compositions of $C_3H_8/N_2/H_2O$ = 1/4/9 at a space velocity of 108,000–170,000 $mL/g_{cat}{\cdot}h$ in the temperature range of 550–650–750 °C. After the SRP reaction, high purity N_2 was fed to the reactor to prevent the unintended coke formation while it is cooled to room temperature. The effluent gases were passed over a cold trap for dehydration, and analyzed by using a gas chromatography (Young Lin Instrument Co, Anyang, Republic of Korea, YL6100 GC) equipped with a Carboxen 1000 packed column to quantify the gaseous components such as H_2, N_2, CO, CO_2, and CH_4 using a thermal conductivity detector (TCD), and GS-GasPro capillary column used to quantify the light hydrocarbons containing C_1–C_3 species. The catalytic activity was compared with conversion of C_3H_8 and product distribution, which was calculated based on the changes in effluent gas concentrations with an internal standard of N_2. Catalytic performances were calculated by the following equations based on the carbon balance in a dry mole basis as described below:

$$C_3H_8 \text{ conversion (mol\%)} = [1 - (\text{number of carbon of propane in products})/(\text{Sum of carbon in gas phase products})] \times 100 \quad (5)$$

$$\text{Specific rate } (h^{-1}) = (\text{converted moles of } C_3H_8/(\text{mols of Ni and Co}){\cdot}h) \quad (6)$$

$$\text{Product distribution (mol\%)} = (\text{mols of the product})/(\text{Sum of product mols in a gas phase}) \times 100 \quad (7)$$

4.2. Characterization of the CA Supports as Well as NCA Catalysts

Powder X-ray diffraction (XRD) patterns of the NCA catalysts were analyzed to validate the crystalline phases and crystallite sizes of the Ni and Co species by using a X'Pert3 Powder (PANalytical) instrument operated with radiation of Cu-Kα of 0.15406 nm at 40 kV and 100 mA in the 2θ range of 10°–80° at a scanning rate of 4°/min. The full width at half maximum (FWHM) values of the metallic Ni-Co peaks at Bragg angles of 2θ = 44°–44.5° were used for the crystallite size calculations with the help of Scherrer's equation by using a Scherrer constant of 0.9 with an assumption of spherical crystals. N_2 adsorption-desorption analysis was performed on a constant volume sorption instrument (Tristar II, Micromeritics) at a temperature of −196 °C after the sample was degassed at the temperature of 350 °C for 4 h in a vacuum condition. The textural properties, such as surface area, pore volume and average pore size of the fresh NCA catalysts were calculated by Brunauer–Emmett–Teller (BET) equation and Barrett–Joyner–Halenda (BJH) model using the desorption branch of N_2 isotherms.

CO chemisorption was carried out to verify the dispersions of the active metals on the NCA catalysts by using an ASAP2020C (Micromeritics) instrument. Initially, 0.2 g of the sample was loaded

in a u-shaped quartz reactor followed by reduction under a flow of 30 mL/min of H_2 at the temperature of 700 °C for 3 h. The reactor was evacuated while it was cooled from 700 °C to the 35 °C for 1 h and kept for an additional 1 h at 35 °C to maintain the vacuum level of 0.02 mmHg. After the leak test, the reduced sample was evacuated for 20 min then analyzed with CO as a probe molecule. CO uptakes were determined by the introduction of CO pulses until the pressure increments of the sample cell were measured. For the calculation of CO chemisorption, the adsorption stoichiometry of H_2 to metals was assumed as one CO molecule per one molecule of the surface metals (Ni and Co).

Temperature programmed reduction with H_2 (TPR) was performed to clarify the reduction behaviors of the fresh NCA catalysts by measuring the consumed amount of H_2 by using a BELCAT-M (MicrotracBEL) instrument. An amount of 30 mg of the sample was loaded in a quartz tube reactor and heated at 500 °C for 1 h under an inert flow of Ar to eliminate contaminants and to clean the catalyst surfaces. After being cooled to 100 °C, 30 mL/min of 10 vol% H_2/Ar was fed to the reactor. After the TCD signal was stabilized after 30 m, the sample was heated up to 1000 °C at a ramping rate of 10 °C/min and H_2 uptakes were measured by TCD after the effluent gases were dehydrated by passing over a molecular sieve 3A trap. Temperature programmed surface reaction (TPSR) of the used NCA catalysts was performed to verify the relative amounts of coke formation on the catalyst surfaces using a BELCAT-M instrument connected with a mass spectrometer (QMS-200, Pfeiffer vacuum, Yong-in, Republic of Korea). 15 mg of the used NCA catalyst was loaded and pretreated under a flow of 30 mL/min of Ar at 500 °C for 1 h in a quartz reactor. After the above pretreatment, the sample tube was cooled down to 50 °C and 10 vol% H_2/Ar was introduced at a flow rate of 30 mL/min. The temperature was increased up to 700 °C at a ramping rate of 10 °C/min to hydrogenate the deposited coke precursors to CH_4, which was detected by collecting a MS signal by measuring the specific fragments such as m/z = 15, which are assigned to the major fragment of CH_4.

To observe the crystalline phases and oxidation states of the Ni and Co species on the reduced and used NCA catalysts, X-ray absorption fine structure (XAFS) analysis with Ni K-edge (8333 eV) and Co K-edge (7709 eV) was performed at 7D beamline located at a Pohang Light Source (PLS). The beamline was equipped with a Si(111) monochromator and ionization chambers to measure the transmitted beam intensity. The powder sample was previously loaded in the reactor, which was positioned between two Ohken ionization chambers filled with N_2 gas for the measurement of incidents and transmitted X-ray intensity. The absorption spectra of the samples, including the NCA catalysts as well as references of NiO, $NiAl_2O_4$, CoO, Co_3O_4 and $CoAl_2O_4$, were recorded with a spectrum of metallic foil. Normalization and XAFS analysis were carried out by using an Athena graphical interface program [41]. Linear combination fitting (LCF) was also performed in the regions of X-ray absorption near-edge structures (XANES) to quantify the crystalline structures of the reduced and fresh NCA catalysts as well.

Supplementary Materials: The followings are available online at http://www.mdpi.com/2073-4344/10/4/461/s1; Figure S1. Textural properties of the fresh NCA catalysts measured by N_2 adsorption-desorption analysis of the (A) adsorption-desorption isotherms and (B) pore size distributions; Figure S2. Wide-angle X-ray diffraction (XRD) patterns of the (A) reduced and (B) used NCA catalysts; Table S1. Catalytic activities of the CA supports with some reference materials.

Author Contributions: K.S.P. and M.H.J. contributed equally. J.W.B. supervised the work, reviewed and edited in writing this manuscript. All authors have read and agreed to the published version of the manuscript.

Funding: This research was funded by the C1 Gas Refinery Program through the National Research Foundation (NRF) grants funded by South Korea (NRF-2020R1A2C2006052 and NRF-2018M3D3A1A01018009).

Conflicts of Interest: The authors declare no conflict of interest.

References

1. Song, C. *Introduction to Hydrogen and Syngas Production and Purification Technologies in Hydrogen and Syngas Production and Purification Technologies*; Liu, K., Song, C., Subramani, V., Eds.; Wiley: Hoboken, NJ, USA, 2009; pp. 1–13.

2. Ghenciu, A.F. Review of fuel processing catalysts for hydrogen production in PEM fuel cell systems. *Curr. Opin. Solid State Mater. Sci.* **2002**, *6*, 389–399. [CrossRef]
3. Hardiman, K.M.; Ying, T.T.; Adesina, A.A.; Kennedy, E.M.; Dlugogorski, B.Z. Performance of a Co-Ni catalyst for propane reforming under low steam-to-carbon ratios. *Chem. Eng. J.* **2004**, *102*, 119–130. [CrossRef]
4. Moon, D.J. Hydrogen production by catalytic reforming of gaseous hydrocarbons (Methane & LPG). *Catal. Surv. Asia* **2008**, *12*, 188–202.
5. Tan, M.; Wang, X.; Hu, Y.; Shang, X.; Zhang, L.; Zou, X.; Ding, W.; Lu, X. Influence of nickel content on structural and surface properties, reducibility and catalytic behavior of mesoporous γ-alumina-supported Ni–Mg oxides for pre-reforming of liquefied petroleum gas. *Catal. Sci. Technol.* **2016**, *6*, 3049–3063. [CrossRef]
6. Ávila-Neto, C.N.; Oliveira, K.D.; Oliveira, K.F.; Arouca, A.M.M.; Ferreira, R.A.R.; Hori, C.E. Interconnection between feed composition and Ni/Co ratio in (La-Ni-Co-O)-based perovskites and its effects on the stability of LPG steam reforming. *Appl. Catal. A Gen.* **2018**, *550*, 184–197. [CrossRef]
7. Li, Y.; Wang, X.; Song, C. Spectroscopic characterization and catalytic activity of Rh supported on CeO_2-modified Al_2O_3 for low-temperature steam reforming of propane. *Catal. Today* **2016**, *263*, 22–34. [CrossRef]
8. Han, J.W.; Kim, C.; Park, J.S.; Lee, H. Highly coke-resistant ni nanoparticle catalysts with minimal sintering in dry reforming of methane. *ChemSusChem* **2014**, *7*, 451–456. [CrossRef]
9. Jóźwiak, W.K.; Nowosielska, M.; Rynkowski, J. Reforming of methane with carbon dioxide over supported bimetallic catalysts containing Ni and noble metal: I. Characterization and activity of SiO_2 supported Ni–Rh catalysts. *Appl. Catal. A Gen.* **2005**, *280*, 233–244. [CrossRef]
10. Lucrédio, A.F.; Assaf, J.M.; Assaf, E.M. Methane conversion reactions on Ni catalysts promoted with Rh: Influence of support. *Appl. Catal. A Gen.* **2011**, *400*, 156–165. [CrossRef]
11. García-Diéguez, M.; Pieta, I.S.; Herrera, M.C.; Larrubia, M.A.; Alemany, L.J. RhNi nanocatalysts for the CO_2 and CO_2+H_2O reforming of methane. *Catal. Today* **2011**, *172*, 136–142. [CrossRef]
12. Park, K.S.; Son, M.; Park, M.-J.; Kim, D.H.; Kim, J.H.; Park, S.H.; Choi, J.-H.; Bae, J.W. Adjusted interactions of nickel nanoparticles with cobalt-modified $MgAl_2O_4$-SiC for an enhanced catalytic stability during steam reforming of propane. *Appl. Catal. A Gen.* **2018**, *549*, 117–133. [CrossRef]
13. Szijjártó, G.P.; Pászti, Z.; Sajó, I.; Erdőhelyi, A.; Radnóczi, G.; Tompos, A. Nature of the active sites in Ni/$MgAl_2O_4$-based catalysts designed for steam reforming of ethanol. *J. Catal.* **2013**, *305*, 290–306. [CrossRef]
14. Han, J.W.; Park, J.S.; Choi, M.S.; Lee, H. Uncoupling the size and support effects of Ni catalysts for dry reforming of methane. *Appl. Catal. B Environ.* **2017**, *203*, 625–632. [CrossRef]
15. Zhang, J.; Li, F. Coke-resistant Ni@SiO_2 catalyst for dry reforming of methane. *Appl. Catal. B Environ.* **2015**, *176–177*, 513–521. [CrossRef]
16. Bian, Z.; Kawi, S. Sandwich-Like Silica@Ni@Silica multicore-shell catalyst for the low-temperature dry reforming of methane: Confinement effect against carbon formation. *ChemCatChem* **2018**, *10*, 320–328. [CrossRef]
17. Li, Z.; Wang, Z.; Kawi, S. Sintering and Coke Resistant Core/Yolk Shell Catalyst for Hydrocarbon Reforming. *ChemCatChem* **2018**, *11*, 202–224. [CrossRef]
18. Wang, C.; Sun, N.; Zhao, N.; Wei, W.; Zhang, J.; Zhao, T.; Sun, Y.; Sun, C.; Liu, H.; Snape, C.E. The properties of individual carbon residuals and their influence on the deactivation of Ni-CaO-ZrO_2 catalysts in CH_4 dry reforming. *ChemCatChem* **2014**, *6*, 640–648. [CrossRef]
19. Kathiraser, Y.; Thitsartarn, W.; Sutthiumporn, K.; Kawi, S. Inverse $NiAl_2O_4$ on $LaAlO_3$–Al_2O_3: Unique catalytic structure for stable CO_2 reforming of methane. *J. Phys. Chem. C* **2013**, *117*, 8120–8130. [CrossRef]
20. Keshavarz, A.R.; Soleimani, M. Optimization of nano-sized Ni/$MgAl_2O_4$ catalyst synthesis by the surfactant-assisted deposition precipitation method for steam pre-reforming of natural gas. *RSC Adv.* **2016**, *6*, 61536–61543. [CrossRef]
21. Zou, X.; Tian, Z.; Wang, X.; Tan, M.; Ding, W.; Lu, X. Formation of magnesium silicate on surface of silica for steam reforming of liquefied petroleum gas. *Catal. Commun.* **2015**, *68*, 116–119. [CrossRef]
22. Park, J.H.; Lee, D.; Lee, H.C.; Park, E.D. Steam reforming of liquid petroleum gas over Mn-promoted Ni/γ-Al_2O_3 catalysts. *Korean J. Chem. Eng.* **2010**, *27*, 1132–1138. [CrossRef]
23. Crisafulli, C.; Scirè, S.; Minicò, S.; Solarino, L. Ni–Ru bimetallic catalysts for the CO_2 reforming of methane. *Appl. Catal. A Gen.* **2002**, *225*, 1–9. [CrossRef]
24. Misture, S.T.; McDevitt, K.M.; Glass, K.C.; Edwards, D.D.; Howe, J.Y.; Rector, K.D.; He, H.; Vogel, S.C. Sulfur-resistant and regenerable Ni/Co spinel-based catalysts for methane dry reforming. *Catal. Sci. Technol.* **2015**, *5*, 4565–4574. [CrossRef]

25. Gao, X.; Tan, Z.; Hidajat, K.; Kawi, S. Highly reactive Ni-Co/SiO_2 bimetallic catalyst via complexation with oleylamine/oleic acid organic pair for dry reforming of methane. *Catal. Today* **2017**, *281*, 250–258. [CrossRef]
26. Tu, W.; Ghoussoub, M.; Singh, C.V.; Chin, Y.-H.C. Consequences of surface oxophilicity of Ni, Ni-Co, and Co clusters on methane activation. *J. Am. Chem. Soc.* **2017**, *139*, 6928–6945. [CrossRef] [PubMed]
27. Kubota, N. Effect of impurities on the growth kinetics of crystals. *Cryst. Res. Technol.* **2001**, *36*, 749–769. [CrossRef]
28. Yuan, Q.; Yin, A.-X.; Luo, C.; Sun, L.-D.; Zhang, Y.-W.; Duan, W.-T.; Liu, H.-C.; Yan, C.-H. Facile synthesis for ordered mesoporous γ-aluminas with high thermal stability. *J. Am. Chem. Soc.* **2008**, *130*, 3465–3472. [CrossRef]
29. Cheng, Z.; Wu, Q.; Li, J.; Zhu, Q. Effects of promoters and preparation procedures on reforming of methane with carbon dioxide over Ni/Al_2O_3 catalyst. *Catal. Today* **1996**, *30*, 147–155. [CrossRef]
30. Natesakhawat, S.; Watson, R.; Wang, X.; Ozkan, U. Deactivation characteristics of lanthanide-promoted sol–gel Ni/Al_2O_3 catalysts in propane steam reforming. *J. Catal.* **2005**, *234*, 496–508. [CrossRef]
31. Natesakhawat, S.; Oktar, O.; Ozkan, U.S. Effect of lanthanide promotion on catalytic performance of sol–gel Ni/Al_2O_3 catalysts in steam reforming of propane. *J. Mol. Catal. A Chem.* **2005**, *241*, 133–146. [CrossRef]
32. Kim, A.R.; Lee, H.Y.; Cho, J.M.; Choi, J.-H.; Bae, J.W. Ni/M-Al_2O_3 (M = Sm, Ce or Mg) for combined steam and CO_2 reforming of CH_4 from coke oven gas. *J. CO2 Util.* **2017**, *21*, 211–218. [CrossRef]
33. Lee, H.Y.; Kim, A.R.; Park, M.-J.; Jo, J.M.; Lee, D.H.; Bae, J.W. Combined steam and CO_2 reforming of CH_4 using coke oven gas on nickel-based catalyst: Effects of organic acids to nickel dispersion and activity. *Chem. Eng. J.* **2015**, *280*, 771–781. [CrossRef]
34. Ewbank, J.L.; Kovarik, L.; Kenvin, C.C.; Sievers, C. Effect of preparation methods on the performance of Co/Al_2O_3 catalysts for dry reforming of methane. *Green Chem.* **2014**, *16*, 885–896. [CrossRef]
35. Shen, K.; Wang, X.; Zou, X.; Wang, X.; Lu, X.; Ding, W. Pre-reforming of liquefied petroleum gas over nickel catalysts supported on magnesium aluminum mixed oxides. *Int. J. Hydrogen Energy* **2011**, *36*, 4908–4916. [CrossRef]
36. Huang, Z.; Wang, X.; Wang, Z.; Zou, X.; Ding, W.; Lu, X. High catalytic performance and sustainability of the Ni/La_2O_3 catalyst for daily pre-reforming of liquefied petroleum gas under a low steam/carbon molar ratio. *RSC Adv.* **2014**, *4*, 14829–14832. [CrossRef]
37. Xu, L.; Zhang, J.; Wang, F.; Yuan, K.; Wang, L.; Wu, K.; Xu, G.; Chen, W. One-step synthesis of ordered mesoporous $CoAl_2O_4$ spinel-based metal oxides for CO_2 reforming of CH_4. *RSC Adv.* **2015**, *5*, 48256–48268. [CrossRef]
38. Han, Y.K.; Ahn, C.-I.; Bae, J.W.; Kim, A.R.; Han, G.Y. Effects of Carbon Formation on Catalytic performance for CO_2 reforming with methane on Ni/Al_2O_3 catalyst: Comparison of fixed-bed with fluidized-bed reactors. *Ind. Eng. Chem. Res.* **2013**, *52*, 13288–13296. [CrossRef]
39. Lobo, L.S.; Figueiredo, J.L.; Bernardo, C.A. Carbon formation and gasification on metals. Bulk diffusion mechanism: A reassessment. *Catal. Today* **2011**, *178*, 110–116. [CrossRef]
40. Amini, E.; Rezaei, M.; Nematollahi, B. Synthesis of mesoporous magnesium aluminate ($MgAl_2O_4$) nanopowder with high surface area with a novel and simple sol–gel method. *J. Porous Mater.* **2015**, *22*, 481–485. [CrossRef]
41. Ravel, B.; Newville, M. ATHENA, ARTEMIS, HEPHAESTUS: Data analysis for X-ray absorption spectroscopy using IFEFFIT. *J. Synchrotron Radiat.* **2005**, *12*, 537–541. [CrossRef]